Temperature-dependent photoluminescence of size-tunable ZnAgInSe quaternary quantum dots*

Qi Ding(丁琪)[1], Xiao-Song Zhang(张晓松)[1,2,†], Lan Li(李岚)[1], Jian-Ping Xu(徐建萍)[1], Ping Zhou(周平)[1], Xiao-Fei Dong(董晓菲)[1], and Ming Yan(晏明)[1]

[1] *Institute of Material Physics, Key Laboratory of Display Materials and Photoelectric Devices, Ministry of Education, Tianjin University of Technology, Tianjin* 300384, *China*

[2] *School of Engineering and Applied Sciences, Harvard University,* 9 *Oxford Street, Cambridge, Massachusetts* 02138, *USA*

(Received 5 February 2017; revised manuscript received 14 March 2017; published online 20 April 2017)

Colloidal ZnAgInSe (ZAISe) quantum dots (QDs) with different particle sizes were obtained by accommodating the reaction time. In the previous research, photoluminescence (PL) of ZAISe QDs only could be tuned by changing the composition. In this work the size-tunable photoluminescence was observed successfully. The red shift in the photoluminescence spectra was caused by the quantum confinement effect. The time-resolved photoluminescence indicated that the luminescence mechanisms of the ZAISe QDs were contributed by three recombination processes. Furthermore, the temperature-dependent PL spectra were investigated. We verified the regular change of temperature-dependent PL intensity, peak energy, and the emission linewidth of broadening for ZAISe QDs. According to these fitting data, the activation energy (ΔE) of ZAISe QDs with different nanocrystal sizes was obtained and the stability of luminescence was discussed.

Keywords: quaternary quantum dots, temperature-dependent photoluminescence, photoluminescence lifetime

PACS: 78.67.Hc, 78.55.–m, 78.40.Fy **DOI:** 10.1088/1674-1056/26/6/067804

1. Introduction

Quantum dots (QDs) have aroused public attention owing to particular photometric characteristics[1–4] which draw applications for light-emitting diodes,[5,6] photovoltaic cells,[7] bio-labeling,[8] QD lasers,[9,10] and photocatalytics.[11] Most luminescent QDs used are commonly II–VI or IV–VI nanocrystals like binary CdSe, CdTe QDs, which contained potential toxic elements.[12–14] Therefore, significant attention has been paid to the new generation of cadmium-free QDs, which are designed and developed for scientific research and application to substitute the heavy metal element included in QDs. A new synthesis method of solution-phase was used successfully to prepare a series of ternary I–III–VI QDs[15] based on $CuInS_2$,[16,17] $CuInSe_2$,[18,19] $AgInS_2$,[20] and $AgInSe_2$[21] QDs, which all show efficient luminescence. To further improve the stability and luminous efficiency of these QDs, new terms of quaternary Zn–I–III–VI QDs[22] with addition of zinc have been receiving increasing attention through an efficient ordinary strategy,[23,24] the optical properties of quaternary ZCIS,[25,26] ZAIS[27] QDs have been reported.

In recent years, several reports about ZAISe QDs[28–30] have triggered much attention because of the stability of selenide. In the literature, the photoluminescence (PL) of ZAISe QDs can be tuned by changing the composition. By controlling the Ag/Zn feed ratio the PL emission could be systematically tuned from 660 nm to 800 nm. The obtained ZAISe QDs have been applied in biomedical imaging successfully.

The temperature-dependent PL can be applied to measure the variation of the emission intensity, peak energy, and emission width of ZAISe QDs with temperature. The experimental results can provide the information about the exciton–phonon coupling, the radiative and nonradiative relaxation processes, and the PL mechanism in ZAISe QDs.

The average phonon energy and the Huang–Rhys factor involved in the variation were derived.[31] Therefore, the temperature-dependent optical properties of ZCIS, Mn:ZCIS, and Ag_2Se[32–34] QDs have been reported. However, there are few previous studies on ZAISe QDs. Therefore it is necessary to investigate the temperature-dependent optical properties of ZAISe QDs.

In this paper, ZAISe QDs with different sizes have been synthesized to finely tune emission wavelength in the visible region. In order to investigate the luminescence mechanism, the temperature dependence of the peak energy, PL intensity, and full width at half maximum (FWHM) are also studied by measuring the temperature-dependent PL spectra of ZAISe QDs. Moreover, the activation energy, the average phonon energy $\langle h\omega \rangle$, and the Huang–Rhys factor S were obtained. The temperature-dependent nonradiative recombination was discussed. Furthermore the small Huang–Rhys factor reflected the internal luminescent mechanism of ZAISe QDs.

*Project supported by the National High Technology Research and Development Program of China (Grant No. 2013AA014201), the National Key Foundation for Exploring Scientific Instrument of China (Grant No. 2014YQ120351), and the Natural Science Foundation of Tianjin (Grant No. 11JCYBJC00300, 4JCZDJC31200, 15JCYBJC16700, and 15JCYBJC16800).

†Corresponding author. E-mail: zhangxiaosong022@126.com

© 2017 Chinese Physical Society and IOP Publishing Ltd

2. Experimental details

2.1. Chemicals

Zinc acetate ($Zn(OAc)_2$, 99.99%), silver acetate (AgOAc, 99.99%), Se powder (99.5%), octadecylamine (OAm, 98.0%), 1-octadecene (ODE, 90%), stearic acid (SA, 99.0%), dodecanethiol (DDT, 98.0%), oleylamine (OA, 99.99%), indium acetate ($In(OAc)_3$, 99.99%) were purchased from Alfa Aesar, methanol, acetone, and chloroform were purchased from Aladdin to synthesize ZAISe QDs.

2.2. Precursor solution

2.2.1. Precursor solution of $Zn(OAc)_2$

A four-neck flask was clamped in a heating jacket to which was added $Zn(OAc)_2$ (0.02195 g), OAm (0.0645 g), and ODE (2.0 mL), with argon put into it throughout. The mixed solution was heated to 160 °C and remained for 10 minutes. The precursor solution of Zn was acquired and reserved at 50 °C for the following supply.

2.2.2. Precursor solution of AgOAc

A four-neck flask was clamped in a heating jacket to which was added 0.0363 g of AgOAc, SA (0.1137 g), and ODE (2.0 mL) with argon put into it throughout. The mixed solution was heated to 160 °C and remained for 10 minutes. The precursor solution of Ag was acquired and reserved at 50 °C for the following supply.

2.2.3. Precursor solution of $In(OAc)_3$

A four-neck flask was clamped in a heating jacket to which was added 0.0584 g (0.1 mmol) of $In(OAc)_3$, 0.2274 g of SA, and 2.0 mL of ODE with argon put into it throughout. The mixed solution was heated to 160 °C and remained for 10 minutes. The precursor solution of In was acquired and reserved at 50 °C for the following supply.

2.2.4. Precursor solution of Se

A four-neck flask was clamped in a heating jacket to which was added 0.0078 g (0.1 mmol) of Se powder, 2 mL of OLA, and 0.1 mL of DDT. The mixture was stir under an argon flow at room temperature until all dissolved.

2.3. Synthesis of ZAISe QDs

The precursor solution of $Zn(OAc)_2$, $In(OAc)_3$, AgOAc, 2-ml DDT, and 6-ml ODE were all taken into a four-neck flask. The reaction mixtures were slowly increased to 180 °C in Argon environment. When the mixture solution became clear, we then injected the Se precursor solution into it and kept the temperature at 220 °C; it reacted for 60 minutes to obtain the ZAISe QDs. We aspirated the solution with different reaction times — 20 min, 30 min, 45 min, and 60 min — under argon, then terminated the reaction immediately by injecting the product into toluene. The untreated ZAISe QDs were purified with methanol and acetone for three times through centrifugation. After that, the purified ZAISe QDs were stored in the chloroform solution.

2.4. Characterization

The PL spectra were measured by the Jobin Yvon FluoroLog-3 fluorescence spectrometer, with a 450-W xenon lamp used as the excitation light source. We obtained the absorption spectra using a Hitachi UV-4100 absorption spectrophotometer. The lifetime of the ZAISe QDs was carried out at Horiba Jobin Yvon FluoroLog-3-time-correlated single-photon counting (TCSPC) fluorescence spectrometer, with a pulsed diode light source (Nano LED) with the wavelength of 367 nm. The morphology and sizes of the ZAISe QDs with different reaction time were performed by HITACHI-HT7700 transmission electron microscopes. The Rigaku D/max 2500v/pc x-ray diffractometer was used to obtain the composition by measuring the phase structure of the QDs. Energy dispersive x-ray spectroscopy spectrum of ZAISe QDs was performed by Hitachi S-8010 scanning electron microscopes equipped with an EDX detector.

3. Results and discussion

The transmission electron microscope (TEM) images of the ZAISe QDs with the different reaction times were shown in Figs. 1(a)–1(d). In the photographs, the average diameters of the ZAISe QDs were estimated to 5 nm, 5.2 nm, 6 nm, and 6.7 nm, respectively. The particles were all spherical in shape. Figure 1(e) shows the energy dispersive x-ray spectroscopy (EDX) spectrum, which displays the composition of the ZAISe QDs. Furthermore, the XRD patterns of the ZAISe QDs with different particle sizes were shown in Fig. 1(f). It is clear that the three diffraction peaks are indexed between the distinct diffraction peaks of cubic ZnSe and chalcopyrite $AgInSe_2$.[28] Due to the ultrafine nature of the nanocrystals, there is an extensive degree of peak broadening in the XRD patterns. There detailed measurement results indicate that the quaternary ZAISe QDs have been synthesized in this experiment.

The normalized PL emission spectra and absorption spectra of the ZAISe QDs synthesized with different particle sizes are plotted in Figs. 2(a) and 2(b), respectively. The corresponding ZAISe QDs exhibit a red shift of emission peak from 647 nm to 694 nm. Due to quantum confinement effect, both the emission and absorption spectra show obvious red shift with the increase of particle size from 5 nm to 6.7 nm. The ZAISe QDs with different particle sizes dispersed in chloroform were excited by an ultraviolet 365-nm LED as shown in Fig. 2(c).

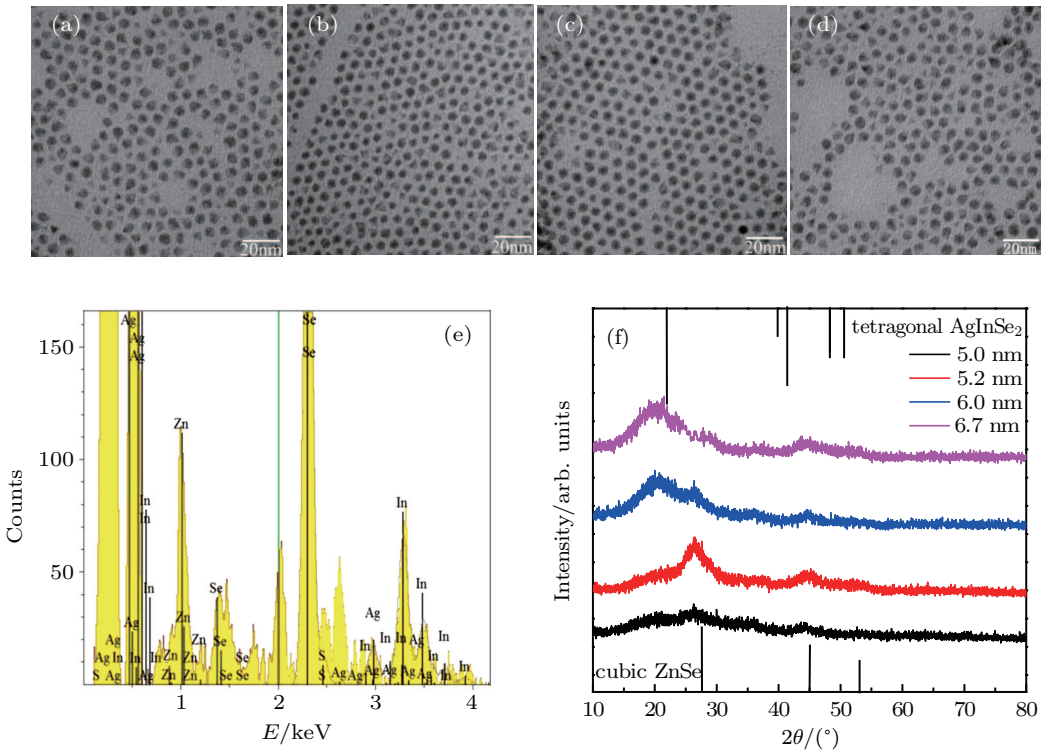


Fig. 1. (color online) TEM images of ZAISe QDs prepared with the reaction time of (a) 5.0 nm; (b) 5.2 nm; (c) 6.0 nm; (d) 6.7 nm. (e) Energy dispersive x-ray spectroscopy spectrum of ZAISe QDs prepared with the particle size of 6.7 nm; (f) XRD patterns of ZAISe QDs with different particle sizes.

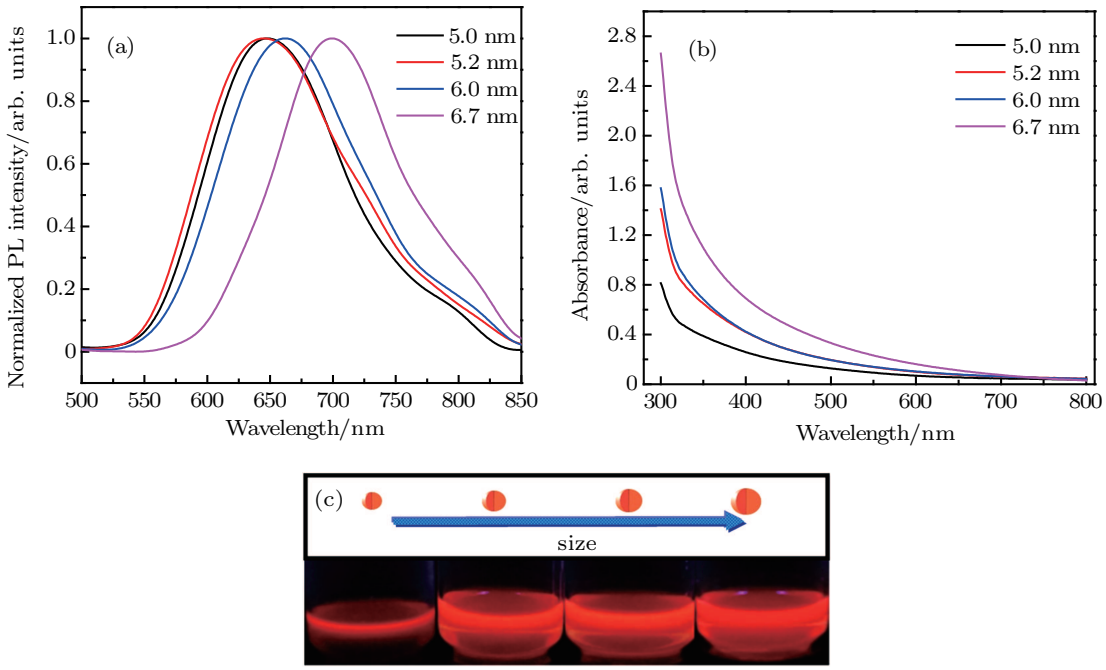


Fig. 2. (color online) (a) Normalized PL emission spectra and (b) UV-vis of ZAISe QDs recorded at different particle sizes. (c) Digital photos of ZAISe QDs with different particle sizes under an ultraviolet spotlight of the 365-nm blue LED (from left to right: 5.0 nm, 5.2 nm, 6.0 nm, and 6.7 nm).

To study the luminescence mechanism, the PL decay curves of the ZAISe QDs excited by an LED with the wavelength of 367 nm are shown in Fig. 3. The monitor wavelengths are 647 nm, 650 nm, 662 nm, and 694 nm respectively. The triexponential function was used to fit PL decay curves of the ZAISe QDs.[31]

$$I(t) = A_1 \exp\left(-\frac{t}{\tau_1}\right) + A_2 \exp\left(-\frac{t}{\tau_2}\right) + A_3 \exp\left(-\frac{t}{\tau_3}\right), \quad (1)$$

where A_1, A_2, and A_3 are the relative weights of the decay component, τ_1, τ_2, τ_3 represent the decay time, respectively.

The fitted results with different particle size are displayed in Table 1. The average lifetime τ_{av} was calculated according to $\tau_{av} = \sum A_i \tau_i^2 / \sum A_i \tau_i$.[32] From the formula we deserved the corresponding average PL lifetimes 234 ns, 247 ns, 254 ns, and 281 ns for ZAISe QDs, which increases with increasing particle size. According to other literature, the medium one of τ_1 may result from the recombination of the conduction band level to a localized intragap level. τ_2 may result from the donor–acceptor pair (DAP) recombination. The shorter lifetime of τ_3 can be attributed to the surface-related radiative recombination.[31] The luminescence mechanism of ZAISe QDs was contributed to by the above three recombination processes. Moreover, the similar tendency was also shown in different particle sizes.

In ZAISe QDs, indium (In_{Ag}) substituted silver site and selenium vacancy (V_{Se}) behave as donors, and silver vacancy (V_{Ag}) behaves as acceptors.[35–39] Therefore, we can reasonably speculate that the PL mechanism of ZAISe QDs includes three forms at room temperature, including conduction band-V_{Ag} recombination, surface-related radiative recombination and DAP recombination.

As shown in Fig. 4, the temperature-dependent PL spectra of ZAISe QDs with different sizes were measured, respectively. The PL intensity was found to decrease as the temperature increased. Moreover, the clear red shift and a linewidth broadening of the emission were also observed.

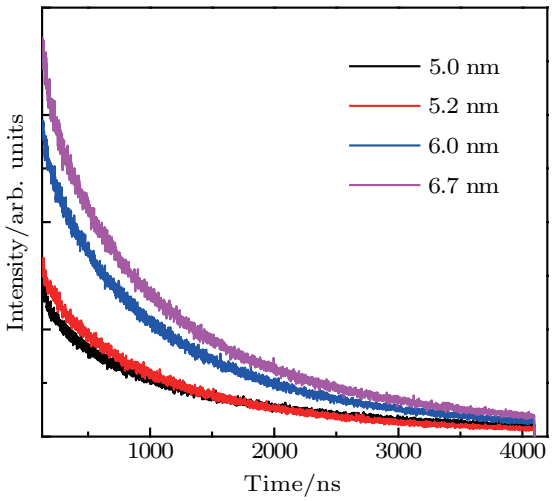


Fig. 3. (color online) PL decay curves of ZAISe QDs with different particle sizes.

Table 1. PL lifetime fitting parameters of ZAISe QDs with different particle sizes.

Particle size/nm	τ_1/ns	A_1	τ_2/ns	A_2	τ_3/ns	A_3
5.0	61.4	6.3	250	93.36	6.29	0.35
5.2	69	7.29	258	92.28	8.13	0.42
6.0	82.2	11.21	289	88.2	9.98	0.59
6.7	57.1	6.09	274	93.31	7.19	0.6

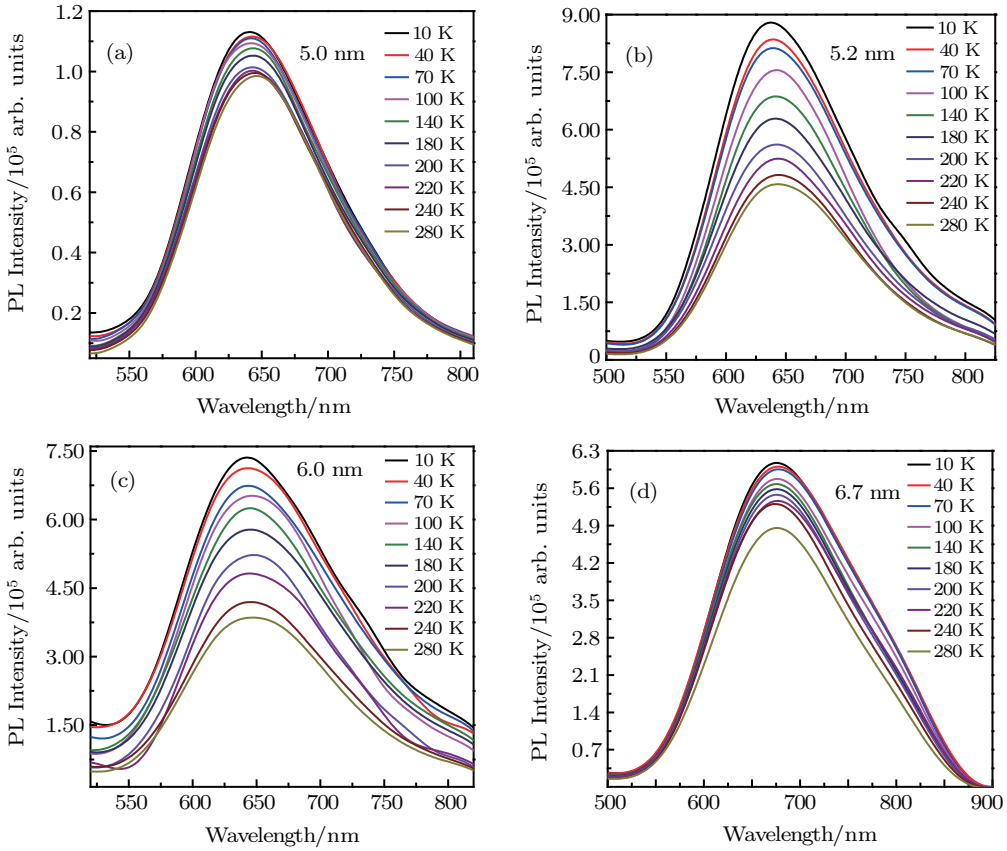


Fig. 4. (color online) Temperature-dependent PL spectra of ZAISe QDs with different particle sizes (a) 5.0 nm; (b) 5.2 nm; (c) 6.0 nm; (d) 6.7 nm.

In order to discern the nonradiative relaxation processes in the QDs, we analyzed the temperature dependence of the PL intensity of ZAISe QDs with different particle size, as shown in Fig. 5. It is clear that the PL intensity decreases with increasing temperature, which is mainly due to thermally activated nonradiative recombination mechanism. The dotted lines represent the actually measured PL intensities and the solid lines represent the fitted curves through Eq. (2)[31]

$$I(T) = \frac{I(0)}{1 + A\exp(-\Delta E/\kappa T)}, \tag{2}$$

where ΔE is the activation energy of the thermal quenching process and $I(0)$ is the emission intensity at 0 K, A is a constant, κ is the Boltzmann constant. These parameters including ΔE and A for the ZAISe QDs are listed in Table 2. It obviously shows that ΔE of ZAISe QDs is much smaller compared with ZnCuInS (115 meV), Mn:ZnCuInS (56.4 meV)[32,33] QDs, suggesting that the nonradiative relaxation process that induced the PL intensity gradually decreases with the increasing temperature. Along with the increasing of the particle size from 5 nm to 6.7 nm, the ΔE increasing indicated the stability of the PL intensity correspondingly.

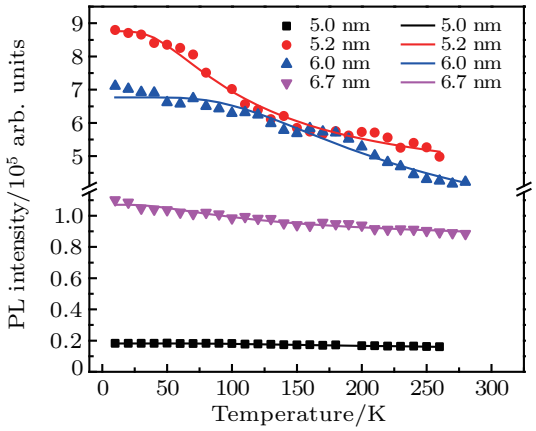


Fig. 5. (color online) PL intensities of ZAISe QDS with different particle sizes as a function of temperature. The solid lines represent fitted curves based on Eq. (2).

Table 2. The fitted parameters of PL intensities of ZAISe QDs.

Particle size/nm	ΔE/meV	A
5.0	15.2	0.31
5.2	17.2	1.54
6.0	31.7	2.53
6.7	44.1	3.57

From the temperature-dependent PL spectra, the variation of peak position of ZAISe QDs with different particle size is shown in Fig. 6. The PL spectra show a clear red shift with the increasing temperature which was induced by the potential of lattice deformation and the exciton–phonon coupling.[40] The values of the energy levels could be fitted from Eq. (3). The results are listed in Table 3. Moreover, those parameters from this equation are involved with the internal interaction in the quantum dots such as the exciton–phonon coupling[31]

$$E_g(T) = E_g(0) - 2S\langle\hbar\omega\rangle\left[\exp\left(\frac{\langle\hbar\omega\rangle}{k_B T} - 1\right)\right]^{-1}, \tag{3}$$

where $\langle\hbar\omega\rangle$ is the average phonon energy, S is Huang–Rhys factor, representing the coupling of exciton transitions to the LO phonon, k_B is the Boltzmann constant. The temperature-dependent fitting values of the $E_g(0)$ are 1.939, 1.932, 1.927, and 1.839 eV respectively proportional to the particle size, which differ from that of ZnCuInS (2.669 eV), Mn:ZnCuInS (1.97 eV).[32,33] Compared to other quaternary QDs, the fitting values of S are between that reported in previous publication such as ZnCuInS (2.1), Mn:ZnCuInS (0.34),[32,33] since the ZnCuInS was induced by the three processes of conduction band to localized intragap level, donor to acceptor recombination and surface related radiative recombination, while the Mn:ZnCuInS was through DAP recombination. It is clear that the ZAISe QDs was induced by the three processes and DAP recombination process is more dominant than that of ZnCuInS. Therefore, the relatively lower coupling of phonon reflected the stability of peak position of ZAISe QDs than other quaternary quantum dots. As shown in Table 3, the decrease of the Huang–Rhys factor means that the coupling of electron–phonon enhances with the increase of particle size, which is caused by the quantum confinement effect.

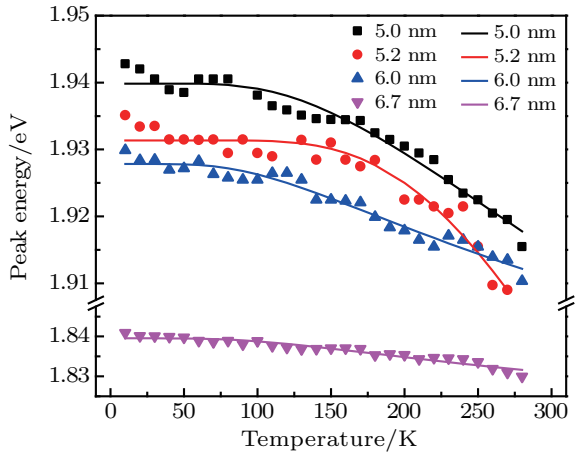


Fig. 6. (color online) Temperature-dependent peak energy for ZAISe QDs with different particle sizes. The fitted curves (full lines) are on the basis of Eq. (3).

The full width at half-maximum (FWHM) of ZAISe QDs with different particle size all increases with increasing temperature, as shown in Fig. 7. As the luminescent mechanism of the QDs was through multi-process, the fitting of line width is significant. The main factors of emission line broadening in ZAISe QDs may be from the carrier to the acoustic phonon mode coupling or from a number of types of emission electrons and holes in the center of the composite. The experimental data were fitted to obtain a better understanding of the

line broadening through Eq. (4), which was always used in majority semiconductor materials to describe the PL spectral broadening,[31] and the fitted results were summarized in Table 4. The broadening of PL peak can be explained as the sum of three patterns, the one is inhomogeneous, the others are because of phonon–exciton and acoustic interactions which represented homogeneous broadening respectively.[31–34,41]

Table 3. The fitting results of temperature-dependent peaks energy of ZAISe QDs with different particle sizes are according to Eq. (3).

Particle size/nm	$E_g(R,0)$/eV	S (Huang–Rhys factor)	$\langle\hbar\omega\rangle$/meV
5.0	1.939	0.048	279.66
5.2	1.932	0.507	23.52
6.0	1.927	0.513	10.06
6.7	1.839	1.088	5.03

$$\Gamma(T) = \Gamma_{\text{inh}} + \sigma T + \Gamma_{\text{LO}}\left[\exp\left(\frac{E_{\text{LO}}}{k_{\text{B}}T}\right) - 1\right]^{-1}, \qquad (4)$$

where Γ_{LO} is the intension of carriers–LO–phonon coupling, Γ_{inh} represents the inhomogeneous line width that is independent temperature, because of the variation of the quantum dots in shape, size, composition, and so on, E_{LO} is the phonon energy of longitudinal optical (LO), and σ represents the carriers acoustic phonon coupling coefficient. Consequently, as the temperature changes from 10 K to 280 K, both the line broadening and the line shift are mainly caused by the exciton to acoustic phonon coupling.[31,32,41] Compared to quaternary ZnCuInS quantum dots,[33] the change trend of these fitting values of the parameters is different, and this may be due to the different particle sizes and nonuniformity of particle sizes of the quantum dot material.[41] In addition, the FWHM of ZAISe QDs increases with increasing particle size from 342.5 meV to 457.6 meV, which was induced by the quantity of defect, more energy level transitions were performed.

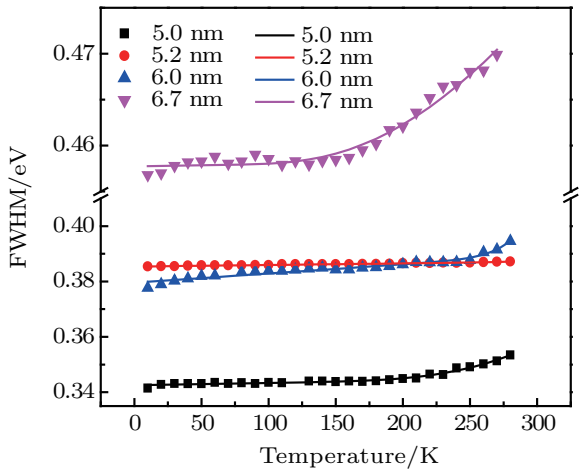


Fig. 7. (color online) Temperature-dependent FWHM of the PL spectra for ZAISe QDs with different particle sizes. The fitted curves (solid lines) are fitted according to Eq. (4).

Table 4. The fitting parameters of temperature-dependent FWHM for ZAISe QDs with different particle sizes.

Particle size/nm	Γ_{inh}/meV	σ/(μeV/K)	Γ_{LO}/meV
5.0	342.5	88.7	369.8
5.2	385.3	55.4	105.3
6.0	389.8	22.1	904.6
6.7	457.6	21.8	188.1

4. Conclusions

The ZAISe QDs with different particle sizes have been successfully synthesized in this paper. By changing the particle sizes, we have successfully tuned the PL of ZAISe QDs. The PL was red-shifted from 647 nm to 694 nm with increasing particle sizes, which depends on the quantum confinement effect. The luminescence mechanism of ZAISe QDs is contributed by the three processes including the conduction-band level to a localized intragap level, the surface-related recombination, and the donor to acceptor recombination from the time-resolved PL study. Through the temperature-dependent emission spectra of ZIASe QDs with different particle sizes, we verified the regular change of temperature-dependent PL intensity, peak energy, and the emission linewidth. Meanwhile, ΔE, $\langle\hbar\omega\rangle$, and S were obtained. In our study, the activation energy (15.2 meV–44.1 meV) is much smaller than the value of ZnCuInS QDs, which indicated that the nonradiative relaxation process that induced the PL intensity slowly decreased with the temperature increasing. The activation energy also increases with the particle size increasing, indicating the stability of the PL intensity correspondingly. The energy gap of QDs is also discussed: the tendency of Huang–Rhys increases with the size of ZAISe QDs which indicates that the coupling of the electron–phonon becomes stronger with the particle size increasing. Moreover, the FWHM of the temperature-dependent spectra is also investigated and analyzed. In addition, the Γ_{inh} of ZAISe QDs are increasing with different particle sizes in a range from 342.5 meV to 457.6 meV, induced by the quantity of defect, and more energy level transitions were performed.

References

[1] Meinardi F, McDaniel H, Carulli F, Colombo A, Kirill A V, Makarov N S, Simonutti R, Klimov V I and Brovelli S 2015 *Nat. Nanotechnol.* **10** 878
[2] Mocatta D, Cohen G, Schattner J, Millo O, Rabani E and Banin U 2011 *Science* **332** 77
[3] Du J, Du Z, Hu J S, Pan Z X, Shen Q, Sun J K, Long D H, Dong H, Sun L, Zhong X H and Wan L 2016 *J. Am. Chem. Soc.* **138** 4201
[4] Regulacio M D and Han M Y 2016 *Acc. Chem. Res.* **49** 511
[5] Yang Y, Zheng Y, Cao W, Titov A, Hyvonen J, Manders J R, Xue J G, Holloway P H and Qian L 2015 *Nat. Photon.* **9** 259
[6] Shirasaki Y, Supran G J, Bawendi M G and Bulovic V 2013 *Nat. Photon.* **7** 13
[7] Lan X, Masala S and Sargent E H 2014 *Nat. Mater.* **13** 233
[8] Shen J, Zhu Y, Yang X and Li C Z 2012 *Chem. Commun.* **48** 3686

[9] Zhao Y, Riemersma C, Pietra F, Koole R, Donega C D M and Meijerink A 2012 *ACS Nano* **6** 9058

[10] Tatebayashi J, Kako S, Ho J, Lwamoto O S and Arakawa Y 2015 *Nat. Photon.* **9** 501

[11] Fernando K A S, Sahu S, Liu Y, Lewis W K, Guliants E A, Jafariyan A, Wang P, Bunker C E and Sun Y P 2015 *ACS Appl. Mater. Interfaces* **7** 8363

[12] Chen O, Zhao J, Chauhan V P, Cui J, Wong C, Harris D K, Wei H, Han H S, Fukumura D, Jain R K and Bawendi M G 2013 *Nat. Mater.* **12** 445

[13] Wuister S F, van Swart I, Driel F, Hickey S G and Donega C D M 2003 *Nano Lett.* **3** 503

[14] Shieh F, Saunders A E and Korgel B A 2005 *J. Phys. Chem. B* **109** 8538

[15] Meinardi F, McDaniel H, Carulli F, Colombo A, Velizhanin K A, Makarov N S, Simonutti R, Klimov V I and Brovelli S 2015 *Nat. Nanotechnol.* **10** 878

[16] Park J and Kim S W 2011 *J. Mater. Chem.* **21** 3745

[17] Li C, Chen W, Wu D, Quan D H, Zhou Z M, Hao J J, Qin J, Li Y W, He Z B and Wang K 2015 *Sci. Rep.* **5** 17777

[18] Zhong H, Wang Z, Bovero E, Lu Z H, Van Vegge F C J M and Scholes G D 2011 *J. Phys. Chem. C* **115** 12396

[19] Yarema O, Bozyigit D, Rousseau I, Nowack L, Yarema M, Heiss W and Wood V 2013 *Nanocrystals Chem. Mater.* **25** 3753

[20] Bai T Y, Li C G, Li F F, Zhao L, Wang Z R, Huang H, Chen C L, Han Y, Shi Z and Feng S H 2014 *Nanoscale* **6** 6782

[21] Kang X, Yang Y, Huang L J, Tao Y, Wang L and Pan D C 2015 *Green Chem.* **17** 4482

[22] Deng D W, Chen Y, Cao J, Tian J M, Qian Z Y, Achilefu S and Gu Y Q 2012 *Chem. Mater.* **24** 3029

[23] Zhang W J and Zhong X H 2011 *Inorg. Chem.* **115** 4065

[24] Zhang J, Xie R and Yang W 2011 *Chem. Mater.* **23** 3357

[25] Yuan X, Zhao J L, Jing P T, Zhang W J, Li H T, Zhang L G, Zhong X H and Masumoto Y 2012 *J. Phys. Chem. C* **116** 11973

[26] Guo W S, Chen N, Tu Y, Dong C H, Zhang B B, Hu C H and Chang J 2013 *Theranostics* **3** 99

[27] Deng D W, Qu L Z, Cheng Z Q, Achilefu S and Gu Y Q 2014 *J. Lumin.* **146** 364

[28] Deng D W, Qu L Z, Zhang J, Ma Y X and Gu Y Q 2013 *ACS Appl. Mater. Interfaces* **5** 10858

[29] Deng D W, Qu L Z, Achilefu S and Gu Y Q 2013 *Chem. Commun.* **49** 9494

[30] Kameyama T, Douke Y, Shibakawa H, Kawaraya M, Segawa H, Kuwabata S and Torimoto T 2014 *J. Phys. Chem. C* **118** 29517

[31] Liu W Y, Zhang Y, Zhai W W, Wang Y H, Zhang T Q, Gu F P, Chu H R, Zhang H Z, Cui T, Wang Y D, Zhao J and Yu W W 2013 *J. Phys. Chem. C* **117** 19288

[32] Zhou P, Zhang X S, Li L, Liu X J, Yuan L L and Zhang X G 2015 *Opt. Mater. Express* **5** 2069

[33] Liu X J, Zhang X S, Li L, Wang X L and Yuan L L 2014 *Chin. Phys. B* **23** 117804

[34] Ji C Y, Zhang Y, Zhang T Q, Liu W Y, Zhang X Y, Shen H Z, Wang Y, Gao W Z, Wang Y D, Zhao J and Yu W W 2015 *J. Phys. Chem. C* **119** 13841

[35] Lee H Y, Song J S, Makino H and Yao T 2002 *Appl. Phys. Lett.* **80** 710

[36] Liu W Y, Zhang Y, Zhao J, Feng Y, Wang D, Zhang T Q, Gao W Z, Chu H R, Yin J Z, Wang Y D, Zhao J and Yu W W 2015 *J. Lumin.* **162** 191

[37] Wang X, Liang Z R, Xu X Q, Wang N, Fang J, Wang J X and Xu G 2015 *J. Alloys Compd.* **640** 134

[38] Jara D H, Stamplecoskie K G and Kamat P V 2016 *J. Phys. Chem. Lett.* **7** 1452

[39] Leach A D P, Shen X, Faust A, Cleveland M C, Croix A D L, Banin U, Pantelides S T and Macdonald J E 2016 *J. Phys. Chem. C* **120** 5207

[40] O'Donnell K P and Chen X 1991 *Appl. Phys. Lett.* **58** 2924

[41] Zhou P, Zhang X S, Liu X J, Xu J P and Li L 2016 *Opt. Express* **24** 19506